Journal of Engineering and Applied Sciences 13 (4): 940-953, 2018
ISSN: 1816-949X

A Comparison of Axisymmetric Models of Multilayer Piezo Actuators for the Creation of Annular Strain Waves

Alexander Vinogradov, Yegor Matveev Yegor, Roman Lubchenko and Pavel Titov
Department of System Analysis, Research Institute of Advanced Materials and Technology, Moscow, Russia

Abstract: This study presents the theoretical results of a comparative analysis of axisymmetric models of piezo actuators with a bimorph and unimorph structures. The unimorph actuator contains ring elements that are fastened to a round metal base. The bimorph actuator has two bound identical piezo ceramic disks with a thin-film electrode between them: the outer surfaces of the disks are covered with thin silver ring electrodes. Different voltages are applied to the ring parts which deforms the bend and creates a system of ring protuberances and depressions. Such actuators are relatively new in piezo engineering-literature does not describe a methodology of their design or comparative analysis. This research is relevant for the choice of an optimal scheme of further development. Quasi-static models are constructed according to the circuits of initiation of bend strains in the multilayer piezoelectric structures (disks, rings and membranes). Special software for their calculation was developed. The results of modeling of bimorphs and unimorphs with ring electrodes were obtained via. the analytical methods and the finite element methods; test models were compared to known designs. The study found that a unimorph with a base with an optimized thickness had greater strains than the bimorph did. Furthermore, the bimorph contained two times as many double-ended electrodes which complicated its structure and limited its application in micropumps without additional protective means which reduce its energy efficiency. As a result, the preferred model is that of a unimorph that serves as a piezo actuator for the creation of annular waves.

Key words: Multilayer piezo actuator, bimorph, unimorph, FEM, membranes, ceramic disks

INTRODUCTION

Piezoelectric actuators based on a unimorph or bimorph are commonly used in micropumps, microvalves and other elements of microfluidics due to their small size and energy consumption and good reliability when operating on various liquid environments. Among all geometric forms of piezo actuators, the workable one is the disk form which has the same bending rigidity and isotropic properties in all radial directions. The physical models of piezo actuators are easy to manufacture which simplifies experimental studies. The mathematical description of the stressed and deformed states of disk and ring piezo actuators uses axisymmetric models that are built in a polar coordinate system (for disks without bends) or a cylindrical system (for bendable membranes).

There are different variants of disk piezoelectric actuators that are used in micropumps (Zhang *et al*., 2016; Pecar *et al*., 2014; Kamitani and Hirata, 2009a, b). The piezo actuators can be unimorph (Anonymous, 2017) or bimorph (Zhang *et al*., 2016) while the piezo pump can be single-chamber (Pecar*et al*., 2014), double-chamber (Hao *et al*., 2015), triple-chamber (He *et al*., 2017; Husband *et al*., 2004) or multi-chamber. The reverse flow can be limited by a cantilever check valve (Anonymous, 2017), a swing-check or vertical-check valve (Zhang *et al*., 2016), a nozzle/diffuser system (He *et al*., 2017); Tesla valves (Forster *et al*., 1995), a network of branch ducts around the outlet (Ma *et al*., 2015), protrusions in the base of the pump chamber (Husband *et al*., 2004), ring-mesa check valves (Anonymous, 2017; Shungo and Takeshi, 2012), etc. The wave of bending strains which carries the fluid can spread in several ways: along the axis in a rectangular (Husband *et al*., 2004) or tubular piezo actuator in a circle in a ring actuator (Bar-Cohen and Chang, 2000) or along the radius in a disk actuator (Kamitani and Hirata, 2009). A fundamental study on microfluidics (Nguyen and Wereley, 2002) described the principle of operation of a peristaltic micropump with round driving membranes and presented an algorithm for calculating the volume of its working chamber and performance.

An important advantage of disk piezo actuators is the possibility of realizing the principle of fluid pumping by running waves of bending strains which propagate

Corresponding Author: Alexander Vinogradov, Department of System Analysis, Research Institute of Advanced Materials and Technology, Moscow, Russia

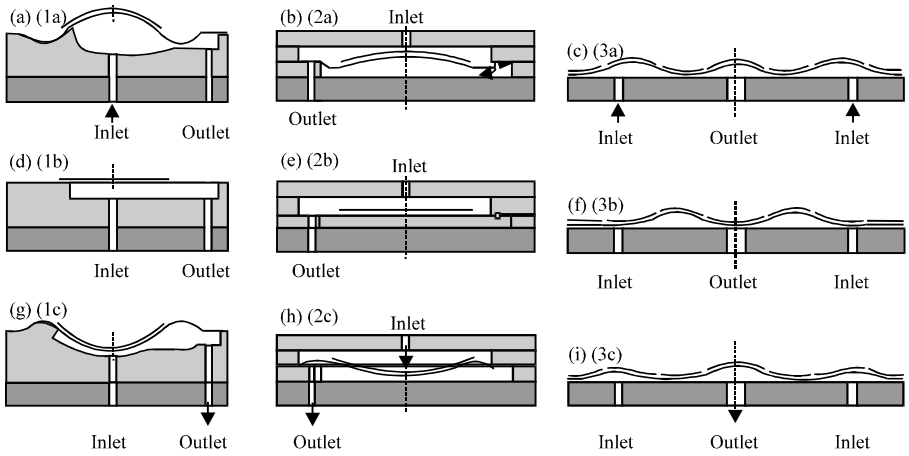

Fig. 1: Disk piezo drives in micropumps (closes analogs): 1) Single-chamber (Dong *et al*., 2007); 2) Double-chamber) (Shungo and Takeshi, 2012); 3) Ring peristaltic (Kamitani and Hirata 2009a, b); a-c) Soaking mode; d-f) Neutral state and g-i) Fischarge mode

from the periphery to the center. A similar design which was considered in patents (Kamitani and Hirata, 2009a, b). Figure 1 is the prototype that is used in this research. The closest analogs of the herein investigated actuator which operated based on the principles of bending strains of a rigid disk are presented in Fig. 1.

The micropump under consideration (Fig. 1) consists of a rigid base (metal or rubber) with five holes (four on the periphery and one in the center) and a disk piezo actuator which is formed by a single disk piezo element with concentrically placed ring electrodes. When signals with a certain phase offset are sent to the piezo elements, the fluid is pumped by the ring sections from the peripheral inlets to the central outlet.

The disadvantages of such a design is the relatively small bend of the disk piezo element during the wavelike ring strain due to increased rigidity. The constant rigidity of the bend of the disk piezo element does not allow increasing the local bend to the necessary size and improving the performance of the micropump. In order to increase the bends, it is necessary to increase the supplied voltage which is not always possible due to the limited electric strength of the piezo material. Another shortcoming of the micropump that is proposed in the prototype is the fact that on drawing near the central part of the body with the outlet, the volume of the chamber with the fluid during a wavelike motion reduces in proportion to the square of the radius which creates excess stress on the piezo disk and breaches the tightness between the ring chambers, this causes uncertainty in regards to the performance because not all of the incoming fluid reaches the outlet. Furthermore, using a bimorph as a bendable disk piezo element requires placing electrodes on both of its surfaces, one of which faces the body chamber and forms a clearance in which the pumped fluid is located which creates the danger of electric breakdown and/or alteration of the properties of the pumped fluid.

This research offers a theoretical framework and results of a modal analysis of designs without the above mentioned flaws.

The purpose of the research is to choose the preferred design of a ring piezoelectric actuator for further development of its structure. The choice was made based on a comparative analysis of axisymmetric models that were built on the basis of a unimorph and bimorph designs which were calculated analytically and numerically via. the Finite Element Method (FEM).

MATERIALS AND METHODS

Literature offers several analytical ways of designing piezoelectric single disks (Samuel, 2011; Li *et al*., 1999; Dong *et al*., 2007) with a limited number of layers and two variants of boundary conditions: with either free bearing or anchorage of the outer duct. In this research, the modeling used an original analytical method of design of multilayer round plates that consisted of multiple concentric ring sections (blocks) with alternating rigidity. The boundary conditions have a wide range of rigid connection with the body of the structure. The method is based on elasticity theory equations (Timoshenko and Gudier, 1979; Timoshenko and Woinowsky-Krieger, 1963) with regard to the inverse piezoeffect (Burdess and

Wren, 1986). The other method that is used in this research to compare the results is the finite element method with the use of a temperature analogy of the piezoeffect.

Theoretical framework of the analytical method of calculation of a multilayer piezo actuator with ring sections with alternating rigidity.

The model under consideration consists of m multilayer ring sections (blocks) with axis z. Strains of an arbitrary layer of a certain block with layers with the same diameter are determined via. Hooke's law equations with regard to the inverse piezoeffect which have the following form in a polar coordinate system (r, θ) (Burdess and Wren, 1986):

$$\xi_r = s_{11}\sigma_r + s_{12}\sigma_\theta + d_{31}E_Z \quad (1)$$

$$\xi_\theta = s_{12}\sigma_r + s_{11}\sigma_\theta + d_{31}E_Z \quad (2)$$

$$\gamma_{r\theta} = 2(s_{11}-s_{12})\tau_{r\theta} \quad (3)$$

$$D_Z = d_{31}(\sigma_r+\sigma_\theta) + \varepsilon_{33}E_Z \quad (4)$$

Where:

ξ_r and ξ_θ = The radial and circumferential linear relative strains

σ_r and σ_θ = The radial and circumferential standard elastic stress

$\gamma_{r\theta}$ = The shear torsional strain

$\tau_{r\theta}$ = The shear stress during the rotation of the layer plane

d_{31} = The transverse piezo module for the piezoelectric layer that is polarized along its depth (the z axis that is perpendicular to the layer plane)

$E_Z = -\partial\Phi/\partial z$ = The strain of the outer electric field with a potential of Φ

D_Z = The induction or density of the charge on the surface of the piezo layer

ε_{33} = The absolute dielectric permeability of the piezo material

The components of the elastic compliance matrix s_{11} and s_{12} are linked with the elastic constants of a transversely isotropic piezo ceramic material with the following Eq. 5:

$$s_{11} = 1/Y,\ s_{12} = -\nu/Y \quad (5)$$

Where:

Y = The Young's modulus

ν = The Poisson's ratio

According to Cauchy equation by Timoshenko and Gudier (1979), linear strains that proceed from Eq. 1 and 2 of the axisymmetric model are linked with radial motion u with the following Eq. 6:

$$\xi_r = \partial u/\partial r,\ \xi_\theta = u/r \quad (6)$$

According to the condition of axial symmetry, motions υ in the circumferential direction θ should equal zero and their derivative $\partial\upsilon/\partial\theta = 0$.

In order to take into account the bend with the displacement of depression w along axis z, it is necessary to consider the problem in a cylindrical coordinate system (r, θ, z). At that, the aforementioned equations remain in force under the condition of absence of axial loads and appropriate normal stress, i.e., $\sigma_z = 0$. Furthermore, the condition of axial symmetry guarantees the absence of all components of shearing stress and angular strains in all the layers of the model (Timoshenko and Woinowsky-Krieger, 1963).

The function of radial motions u depends on two linear coordinates r and z which is why in a cylindrical system, it as the form of u = u(r, z).

Based on Eq. 1 and 2, radial motions with regard to Eq. 5 and 6 are expressed with the following equation as two-variable functions:

$$\sigma_r(r, z) = \left[Y/(1-\nu^2)\right]\left[\partial u/\partial r + \nu(u/r) - (1+\nu)d_{31}E_Z\right] \quad (7)$$

$$\sigma_\theta(r, z) = \left[Y/(1-\nu^2)\right]\left[\partial u/\partial r + \nu(u/r) - (1+\nu)d_{31}E_Z\right] \quad (8)$$

The main differential equation of equilibrium for the axisymmetric problem has the following form (Timoshenko and Woinowsky-Krieger, 1963):

$$r\times(\partial\sigma_r/\partial r) + \sigma_r - \sigma_\theta = 0 \quad (9)$$

which with regard to Eq. 7 and 8, comes down to a second order differential equation in partial derivatives with respect to the desired function u(r, z):

$$\partial\left[(1/r)\times\partial(ur)/\partial r\right]/\partial r = 0 \quad (10)$$

Double integration with regard to the Kirchhoff hypothesis about the linearity of standards solves Eq. 10 in the following form:

$$u(r, z) = (C_1 - C_2 z)r + (C_3 - C_4 z)/r \quad (11)$$

While arbitrary constants C_1-C_4 for each multilayer block are determined from the boundary conditions. Internal forces that are attributed to the perimeter of the circle of radius r: axial radial forces $N_j(r)$ and bending moments $M_j(r)$ are integrally characterized by intensiveness of the following form:

$$N_j(r) = \int_0^H \sigma_{rj}(r, z)dz$$
$$M_j(r) = \int_0^H \sigma_{rj}(r, z)zdz \quad (12)$$

Where:

$H = h_1 + h_2 + \ldots, h_n$ = The total thickness of the model

z-coordinate = The reckoned from the lower surface of the first bottom layer

The bending function is found using the following Eq. 13:

$$w(r) = C_2 r^2/2 + C_4 \ln(r) + C_5 \quad (13)$$

The angular displacement of the standard with a bend of $\varphi(r)$ = -dw/dr through the integration constants equals:

$$\varphi(r) = -C_2 r - C_4/r \quad (14)$$

If in the m block model, the j block number is reckoned from the first one that contains an axis of symmetry, then for strain-stress state functions in block j, analytical dependencies contain five unknown constants C_{1j}, C_{2j}, …, C_{5j}. Boundary conditions and finding unknown constants. The problem has a total of 5 m unknowns.

In the first solid block (without a hole) which contains an axis of symmetry (j = 1), the angular displacement of standard φ_1 and the radial motion u_1 equal zero at r = 0. Then, $C_{41} = C_{31} = 0$. The remaining 5 (m-2) constants are found from the boundary conditions of block conjunction and fixation of the outer surface.

In the m model, there is one boundary between the blocks. The conjunction conditions on the boundaries with the outer radiuses R_j and inner radiuses R_{j-1} of static and kinematic strain-stress state functions (a total of five types) enable obtaining 5(m-1) linear equations with respect to the sought unknowns C_{1j}-C_{5j} ($j \neq 1$ for C_{3j} and C_{4j}). These equations are as follows:

$$N_j(R_j) = N_{j+1}(R_j)$$
$$M_j(R_j) = M_{j+1}(R_j)$$
$$u_j(R_j, 0) = u_{j+1}(R_j, 0)$$
$$u_j(R_j) = u_{j+1}(R_j)$$
$$\varphi_j(R_j) = \varphi_{j+1}(R_j) \quad (15)$$

Here, j = 1, 2, 3, …, m-1. The other three equations are composed from the boundary conditions on the outer surface of the multilayer model at $r = R_m$:

$$M_m(R_m) + K_M \times \varphi_m(R_m) = 0$$
$$N_m(R_m) + K_N \times u_m(R_m, z_s) = 0$$
$$w_m(R_m) = 0 \quad (16)$$

Where:

K_M = The rigidity of the elastic coupling of the model surface with the base for the turn

K_N = The rigidity of the elastic coupling of the surface for the radial motion

z_s = The coordinate of the point of attachment of the outer surface to the base

All three parameters are set during modeling. Extreme cases are as follows:

- If $K_M = K_N = 0$, then the model has free bearing on a smooth surface
- $K_M = K_N \to \infty$, an anchorage of the outer surface is modeled
- $K_M = 0$, $K_N \to \infty$, a hinged bearing is modeled
- $K_M \to \infty$, $K_N = 0$, a slotted bearing is modeled

In other cases, the elasticity is assessed experimentally. This forms and solves a system of 5 (m-2) linear equations with respect to the same number of unknown constants.

The found constants and Eq. 11 and 13 are used to determine displacements in each ring block. Stress is calculated based on the following Eq. 17 and 18:

$$\sigma_{rj}(r, z) = \left[Y/(1-v)\right]\left[\begin{matrix}(C_{1j} - C_{2j}z) - (1v)/(1+v) \times \\ (C_{3j} - C_{4j}z)/r^2 - \beta U\end{matrix}\right] \quad (17)$$

$$\sigma_{\theta j}(r, z) = \left[Y/(1-v)\right]\left[\begin{matrix}(C_{1j} - C_{2j}z) + (1-v)/(1+v) \times \\ (C_{3j} - C_{4j}z)/r^2 - \beta U\end{matrix}\right] \quad (18)$$

Here, coordinates r and z as well as the elastic characteristics are taken in accordance with the block number j and layer number i; $\beta = d_{31}/h_i$ is the piezoelectric coefficient of linear strain, U is voltage in the piezo element.

In order to implement the method, we developed special software that included the "pk2016" computation module, a database with the properties of the materials and a file with the parameters of the computational model. The interactive graphical interface of the program displays the modeling process and allows adjusting the physical and geometric properties of the model, setting voltage on the piezo elements and saving the current parameters of the model and the results in files.

The described method is easy to adapt to computing temperature strain and stress. To that end, it is sufficient to add the temperature element in the form of $\alpha \times dT$ where dT is temperature changes and α is the temperature coefficient of linear expansion, to summands $d_{31}E_Z$ in the initial Eq. 1 and 2 and subsequent Eq. 7 and 8 and to summands βU in Eq. 17 and 18.

RESULTS AND DISCUSSION

Model of a bimorph actuator with ring electrodes: Figure 2 shows a flowchart of a bimorph axisymmetric piezo actuator with ring electrodes. It includes two piezoelectric disks (bimorph) each with a thickness of $h_p = 0.2$ mm, rigidly connected between each other with a metallized layer. The flat surfaces of the bimorph have silver ring electrodes $h_e \cong 5$ μm thick.

The outer diameter of electrode i equals: $D_i = 10i$ mm ($i = 1, 2, \ldots, 5$); clearance $\delta = 1$ mm. The thickness of outer electrodes is ignored during the first approximation, since, $h_e << h_p$. The bimorph is rigidly attached along the outer cylindrical surface of the radius $R_5 = 25$ mm. The arrows that point upwards show the vectors of initial polarization P_0 in each layer of the bimorph.

Power sources supply alternating current U_i to the electrodes which changes during time t according to the harmonic law:

$$U_i(t) = U_0 \cos\left[\omega t + \Delta\varphi(i-1)\right] \quad (19)$$

With an amplitude of U_0, circular frequency ω and phase displacement $\Delta\varphi$. Figure 2 shows an example of a bimorph with five electrodes and the first and fifth electrodes have identical potentials from source U_1 at that which corresponds to the phase displacement between neighboring electrodes $\Delta\varphi = 90°$. The electrode that connects the piezo ceramic disks has zero potential.

If the amplitude equals $U_0 = 80$ V, then at the initial point in time $t_0 = 0$, regardless of the frequency, according to Shungo and Takewshi (2012), the voltages on the electrodes will be:

$$U_1 = U_5 = +80 \text{ V}; U_2 = U_4 = 0; U_3 = -80 \text{ V} \quad (20)$$

The difference of potentials between the main and zero electrodes (voltage U_i) is considered positive when the electric field intensity vector $E = U/h_p$ matches the direction of vector P_0 of the initial polarization of the piezo element (Fig. 2). In case of a matched connection, the lower ring sections with positive, according to Timoshenko and Gudier (1979), potentials ($U_1 > 0$ and $U_5 > 0$) are reduced in terms of their planar sizes while the upper sections with opposite connection (arbitrarily $U_1' < 0$ and $U_5' < 0$) expand. Such strains bend these sections upwards. In order to model both layers of the bimorph, we used PZT-5H piezo ceramics with the following properties:

- Elasticity modulus $Y_p = 60.6$ GPa
- Poisson's ratio, $\nu_p = 0.29$
- Transverse piezo modulus d31 = –2.74·10-7 mm/V;
- Piezoelectric coefficient of linear expansion

$$\beta = d_{31}/hp = -1.37 \times 10^{-6} (1/V)$$

The calculation was performed through the method of temperature analogy using the ANSYS V. 15

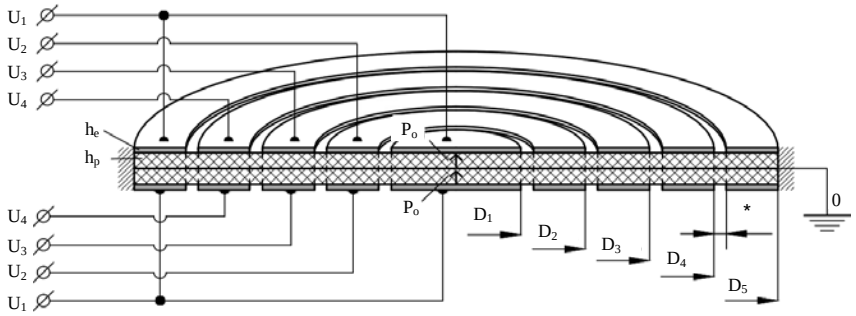

Fig. 2: Flowchart of a bimorph disk actuator with five electrodes

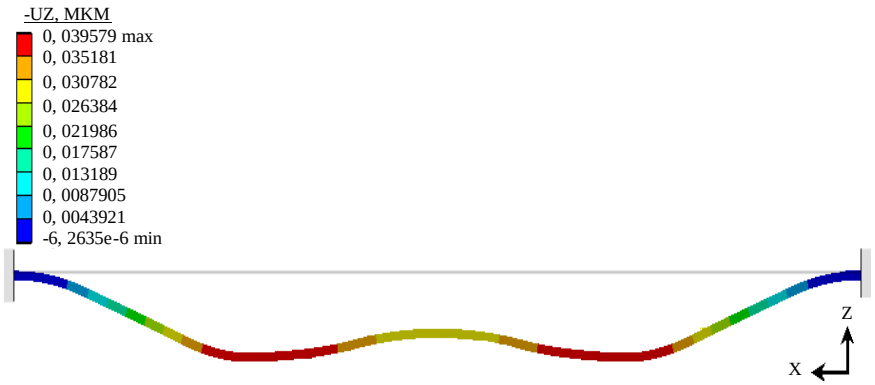

Fig. 3: Map of vertical displacements UZ of the bimorph piezo actuator

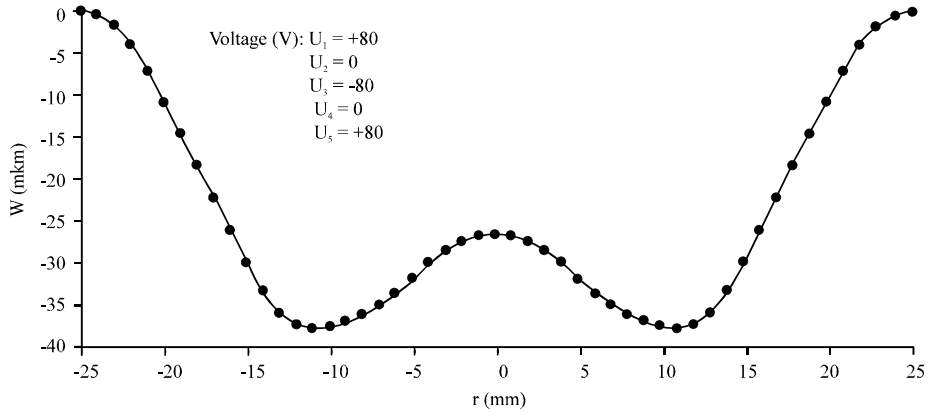

Fig. 4: Strain of a bimorph with five pairs of ring electrodes. Strains are shown for the bottom layer at t = 0 and $\Delta\varphi = 90°$

Program. The condition of analogy is the equivalence of free piezoelectric and temperature strains in the plane of the piezo ceramic plate:

$$d_{31}U/h_p = \alpha T^\circ$$

Therefore, instead of voltages U_i, temperatures T_i° are set in the model which are different in upper and lower signs (i = 1, 2, 3, 4, 5) while the temperature coefficient of linear expansion α is taken as equal to β (with regard to the sign):

Electrode	i =	1	2	3	4	5
Up	T_i° =	–80	0	+80	0	–80
Down	T_i° =	+80	0	–80	0	+80

Figure 3 shows a map of vertical displacements. One can see that the bend of the structure runs downwards with the formation of a saddle in the central part. Maximum vertical displacement UZ (W_{max}) is 39.6 μm. At the same time, the maximum bend W_{max} was 39.39 μm according to analytical calculations.

The analytically obtained graphical dependency of the bimorph strain is shown in Fig. 4. We also determined the form of the elastic curve in the axial section of the deformed disk bimorph piezo actuator when voltage that altered according to the cosine law was supplied to each ring element.

The finite-element model simulated the operation of the bimorph during a time period t from 0-12 sec with a step of 1 sec. One transverse wave with a period of $T = 2\pi/\omega$ propagates from the periphery to the center of the pump during the time under consideration. Circular frequency ω which equals the rate of phase change of the wave process fluctuations in time, during 1 sec is $\pi/6$ (i.e., $\omega = 0.5236$ rad/sec = 30°/sec). The initial level of the voltage at time point t = 0 is U_0 = 80 V. Phase shift between two neighboring elements $\Delta\varphi = \pi/2$ (1.57 radian or 90°). The current level of voltage at I piezo element (i = 1, ..., 5) at time point t is determined from Eq. 19.

Figure 5 shows the dependency of the phase time t on the current voltage U_i which is supplied to i pair of electrodes (i = 1, ..., 5) that are part of the top and bottom layers of the disk piezo bimorph. At that one second of phase time corresponds to 30° phase change.

Figure 6 shows the form of elastic curves during the strain of the disk piezo bimorph which correspond to each moment of phase time. The diagram shows the downward displacement of the membrane (depicted with a sold line),

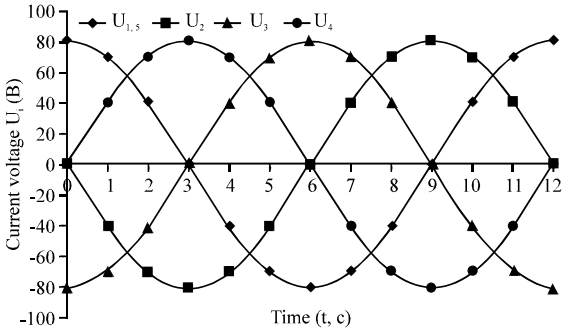

Fig. 5: Forms of signals that are sent to the top and bottom layers of the disk piezo bimorph

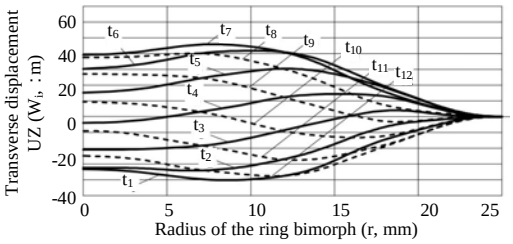

Fig. 6: Form of the elastic curve of a strained bimorph at time points t_1 = 1 sec, t_2 = 2 sec, ..., t_{12} = 12 sec (t_0 = 0). Phase step π/6

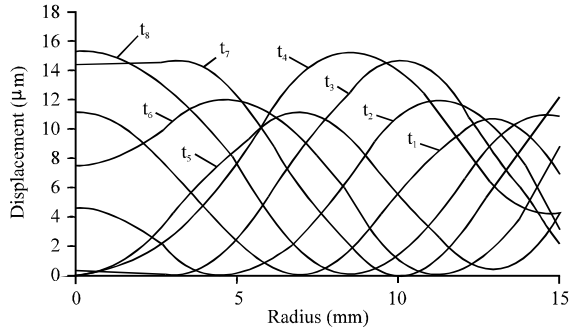

Fig. 7: Analog (Kamitani and Hirata, 2009a). Diagrams of membrane displacements along the radius at various time points t_1, …, t_8. Phase step π/4

t = 1, ..., 6 sec and the upward displacement of the membrane (depicted with a dotted line), t = 7, ..., 12 sec. One can see that the direct and reverse forms of the elastic curve do not match. The maximum value that was calculated for 12 time points was UZ_{max} = 45.7 μm while the minimum one was UZ_{min} = -39.9 μm.

Figure 7 shows similar graphical dependencies of the bend on the radius of a membrane with a diameter of 30 mm for eight time points which are indicated in patent (Samuel, 2001).

The minimums of all dependencies are formally reduced to zero value which is incorrect, since in this case as seen from the diagrams, the boundary conditions of rigid attachment of the outer surface of the plate are violated, namely: with a radius of 15 mm, all curves show the values of displacements and their derivatives on the outer surface of the plate which differ significantly from zero.

Therefore, we considered a case when the wavelike transverse strain of the piezo bimorph was restricted on one side by the bottom of a 20 μm deep chamber. At that, we solved a specific problem of determining force P which was distributed across the contact circumference of radius a, the value whereof was found through the iteration method.

The integral reaction force P which is distributed across the circumference of radius a creates an additional bend W(r) of the entire plate with a rigidly connected surface of radius R. The intensity of the distributed shearing load on the contact line is p = P/(2πa). The bend function is determined via. the following algorithm (Timoshenko and Gudier, 1979; Timoshenko and Woinowsky-Krieger, 1963). At 0≤r≤a:

$$w_1(r) = P/(16\pi D)\times\left[\begin{matrix}2\left(a^2+r^2\right)\ln\left(a/R\right)+\\ \left(r^2/R^2+1\right)\left(R^2-a^2\right)\end{matrix}\right]$$

and at a<r≤R:

$$w_2(r) = P/(16\pi D)\times\left[\begin{matrix}2\left(a^2+r^2\right)\ln\left(r/R\right)+\\ \left(a^2/R^2+1\right)\left(R^2-r^2\right)\end{matrix}\right]$$

Here, D is the cylindrical rigidity of the round plate. For a transversely isotropic homogenous plate which a bimorph disk can be regarded as without regard to the electrodes, the cylindrical rigidity is determined from the following equation:

$$D = Yh^3/\left[12\left(1-v^2\right)\right]$$

Where:
Y = Young's modulus
v = The Poisson's ratio
h = The full thickness of the plate

In the case of a multilayer plate (or block) containing n layers, an equivalent unit cylindrical rigidity is used which is found from the following equation:

$$D^* = \frac{1}{3}\sum_{i=1}^{n}\frac{Y_i}{1-v_i^2}\left[\left(z_i-\delta\right)^3-\left(z_{i-1}-\delta\right)^3\right]$$

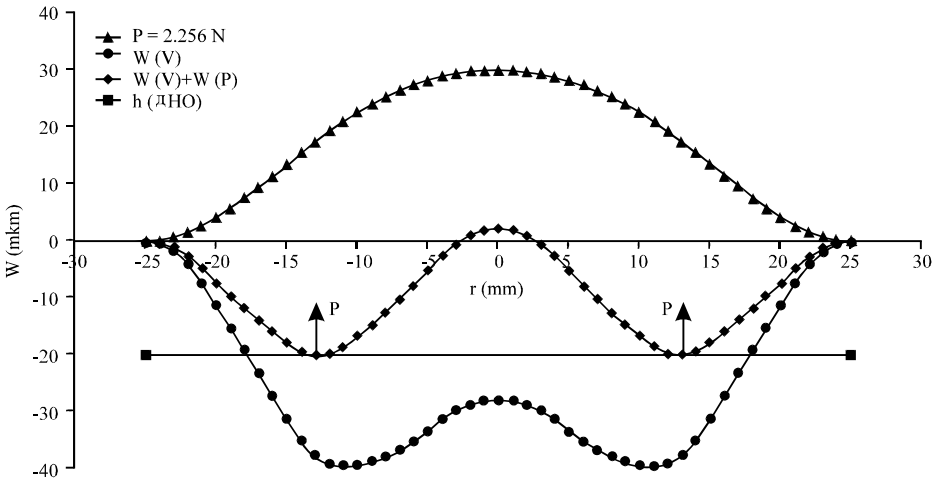

Fig. 8: Bimorph bending under different loadings; Bimorph bending; Phase 0. Number of electrodes -5

Here, Y_i and ν_i are Young's modulus and Poisson's ratio, respectively, of layer i, z_{i-1} and z_i are coordinates of the lower and upper boundaries of layer i on the z-axis, along which depressions W are calculated, δ is the coordinate of the neutral surface of the multilayer system which is found from the following equation:

$$\delta = \sum_{i=1}^{n} \frac{E_i h_i \delta_i}{1-\nu_i^2} \Big/ \sum_{i=1}^{n} \frac{E_i h_i}{1-\nu_i^2}$$

where, $\delta_i = (z_{i-1} + z_i)/2$ is the coordinate of the middle plane of layer i with a thickness of h_i. This algorithm was used to determine the force of vertical reaction of the bottom of the chamber P = 2.256 N which was required to lift the bent surface of the bimorph to the level of the chamber depth (h = 20 μm) and find the radius of the contact circumference a = 13 mm.

Figure 8 shows the diagrams of bending of a round bimorph plate with a diameter of 50 mm and a thickness of 0.4 mm which was made out of PZT-5H piezo ceramics with different loading types.

The upper curve "P = 2.256 N" shows the form of the plate bend from the effect of force P which is distributed evenly across the narrow ring of radius a = 13 mm. The second curve "W(V)" which lies in the range of negative values of the bend, illustrates the form of strain of the bimorph only from the piezoelectric impact at set voltages (Eq. 20). As seen from this dependency, the minimums of functions are located at points with the abscissa r_m = 11 mm. The third curve "W(V)+W(P)" is a sum of the two first dependencies and shows the actual profile of the strained surfaces of the bimorph membrane. The straight segment "h" shows the bottom of the base chamber.

It was found that the minimums of the resulting bending function were displaced from the axis of symmetry (a>rm in this case by 2 mm) towards the fastened surface. The shape of the resulting profile of the bimorph changed somewhat when compared to free strain. Nullifying the minimums of bending while preserving the boundary conditions of rigid connection of the membrane on the outer surface would be impossible at any reasonable level of contact force.

In most cases, transverse displacements are calculated without regard to the electrodes. However, the studies showed that the rigidity of electrodes has a considerable effect on the bending of the disk piezo bimorph. We examined a model, in which electrodes with a thickness of he = 5 μm were placed on the upper and lower surfaces of rings. The intermediate layer of metallization was not taken into account, since, it virtually is not deformed during bending. The electrodes were made of silver and has Young's modulus of Y_{Ag} = 82.7 GPa and Poisson's ratio ν_{Ag} 0.37. The maximum bending for the model with electrodes which was calculated according to the FEM was 35.8 μm, i.e., 9.6% less than in the model without electrodes (39.6 μm) which is indicative of the need to take electrodes into account when designing high-accuracy piezo actuators.

Model of a unimorph actuator with ring piezo elements: We considered a model that consisted of a single active piezoelectric layer that was rigidly connected with an elastic base layer (unimorph). The flowchart of the unimorph model is presented in Fig. 9.

The active layer with a thickness of h_p = 0.2 mm was made out of PZT-5H piezo ceramics with the same

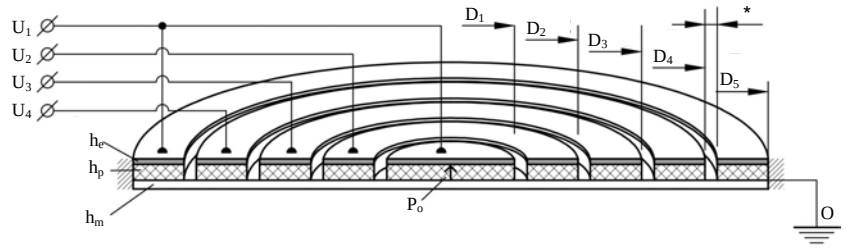

Fig. 9: Flowchart of a unimorph with five ring piezo elements

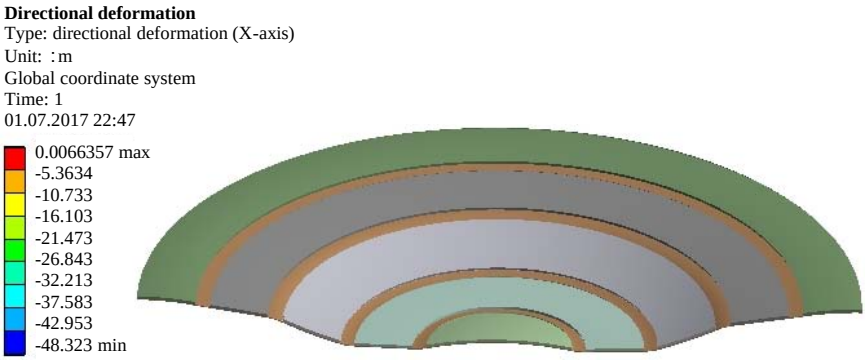

Fig. 10: Map of vertical displacements UZ of the piezo unimorph

properties as those used in the bimorph model. The elastic layer had a thickness of h_m = 0.06 mm and was made out of L63 brass with the following properties: Young's modulus Y_m = 114.0 GPa, Poisson's ratio v_m = 0.36. The connection was rigid, along the side surface of the unimorph. Voltages that were supplied to the ring sections of the active layer were as follows:

$$U_1 = U_5 = -80 \text{ V}, U_2 = U_4 = 0 \text{ V}, U_3 = +80 \text{ V}$$

The calculation was performed through the method of temperature analogy using the ANSYS V. 15 Program. Therefore, respective temperatures Tj were set instead of voltages U_j and the temperature coefficient of linear expansion was taken as α = -1.37×10-6 (1/°C).

The outer diameter of element i equals: D_i = 10i mm (i = 1, 2, …, 5); clearance δ = 1 mm. The thickness of external electrodes is not taken into account, since, $h_e << h_p$. The unimorph is rigidly connected to the outer cylindrical surface of radius R_5 = 25 mm.

Figure 10 shows a map of vertical displacements of the piezo unimorph without regard to the thickness of the electrodes. One can see that the structure is bent downwards with a formation of a local protuberance in the central part, similar to the bimorph piezo drive that was considered above. Maximum vertical displacement in the negative direction-UZ (W_{min}) was 48.32 μm which was 22% greater than that of the bimorph (39.6 μm).

When taking into account the thickness of the electrodes (h_e = 5 μm) which are located on the surfaces of the piezoelectric layer, the bend is reduced by 13.4% in relation to the model without electrodes and is 41.8 μm.

Analytical comparison of models: In order to compare the characteristics of transformation of the electric tension in the deformation, we calculated the bimorph and unimorph models of actuators according to the developed method with an implementation in the PK2016 Program. The main criterion of comparison is the size of the depression W. At different points in time, the voltages that determined the current phase ωt were set according to Eq. 19 with a step of 15°. The amplitude was U_0 = 80 V, phase shift was 90°.

Figure 11 shows the shapes of the bands of two models at the initial moment when the current phase is ωt = 0. The bottom part of figure shows a fragment of the program window with a scheme of the unimorph. In the rectangles that represent the sections of piezoelectric rings, symbols "+" and "-" denote the sings of supplied voltages.

The greatest negative depression W_{min} for the bimorph is -39.39 μm with a radius of 11 mm while for the unimorph, it is -47.91 μm with a radius of 6 mm. The difference between this result and that of the finite element method does not exceed 1%.

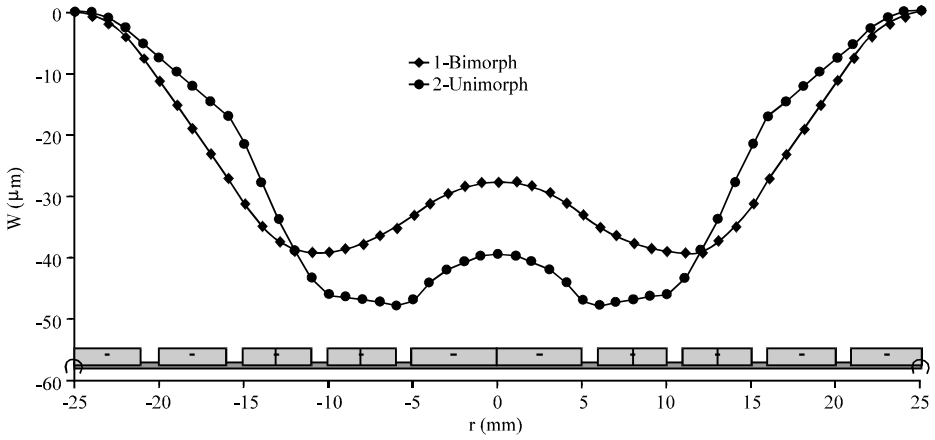

Fig. 11: Bend shape (1 phase wt. = 0): 1-bimorph, 2-unimorph. Bottom part-unimorph scheme from the PK2016 Program

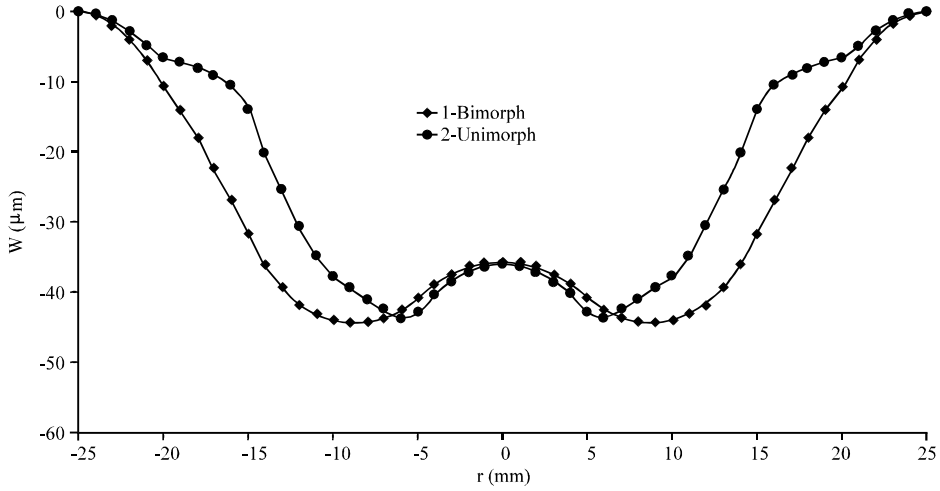

Fig. 12: Depressions (2 phase wt. = 15°): $W_{min}1$ = -44.36; $W_{min}2$ = -43.89 µm

Figure 12 shows similar dependencies for the second phase wt. = 15° which shows that the maximum negative depressions of both models are virtually identical.

Figure 13 shows the distribution of depressions for the fourth phase wt. = 45° for the same models without regard to the electrodes (curves 1 and 2 in two-layer models) and with regard to silver electrodes with a thickness of 5 µm and a solder alloy layer with a thickness of 10 10 µm (curves 3 and 4 in five-layer models). One can notice that the shapes of dependencies W(r) in the models differ considerably. Thanks to the better flexibility of ring sections without piezo ceramics, the unimorph has a better ability to form annular waves than the bimorph does.

The presence of electrodes on two sides of the piezo ceramics and the binding solder allow layer between the brass base and the piezo ceramics reduces the theoretical depression of the unimorph by 11% while the consideration of the three layers of electrodes in the bimorph reduces its depression by 12%.

Figure 14 and 15 show schemes of five-layer computation models and present the diagrams of depressions W(r) of the bimorph and unimorph actuators with regard to electrodes with a phase offset of 180° of the control voltage with an amplitude of ±80 V.

As one can see, the depressions of the unimorph are generally somewhat larger than those of the bimorph are. Furthermore, the distribution of the wavelike deformation of the unimorph is more contrasting. This is determined by the presence of ring sections with lower rigidity in clearances between piezo elements in the model (Fig. 15) which is lacking in the bimorph model, the high rigidity whereof is determined by two solid piezo ceramic disks (Fig. 14).

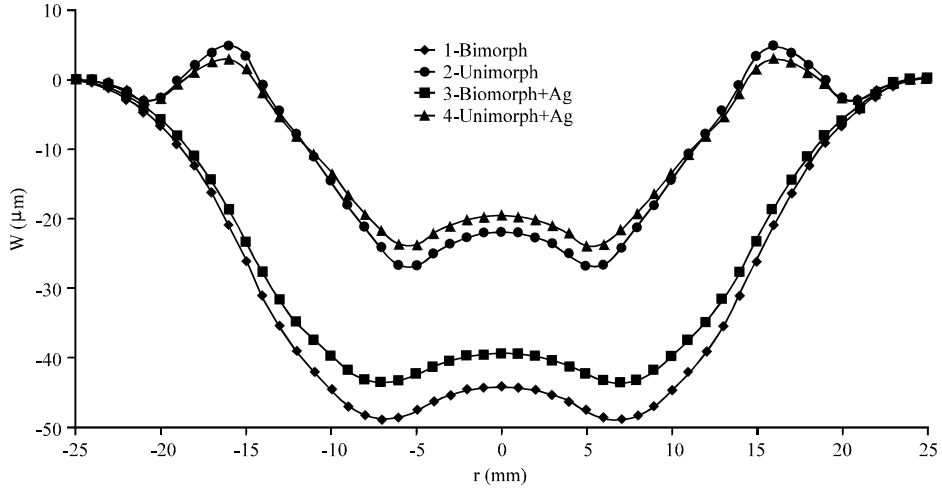

Fig. 13: Depressions of the bimorph and unimorph models at the fourth phase wt. = 45°. 2-layer without electrodes: $W_{min}1$ = -48.81; $W_{min}2$ = –27.0 μm; five-layer with Ag electrodes: $W_{min}3$ = -43.58; $W_{min}4$ = -24.3 μm

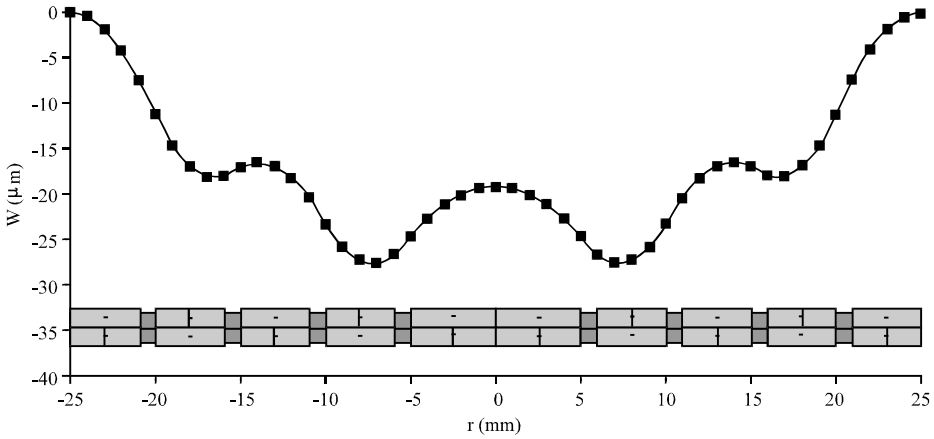

Fig. 14: Scheme and depressions of the bimorph. Phase wt. = 0, phase offset Δφ = 180°. Extreme W_{min} = -27.69 μm at r = 7.3 mm

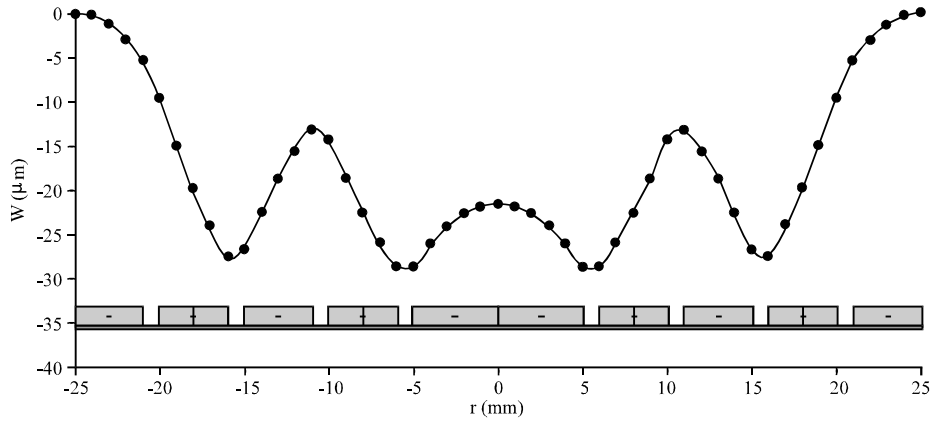

Fig. 15: Scheme and depressions of the unimorph. Phase wt. = 0. Phase offset Δφ = 180°. Extreme W_{min} = -29.36 μm at r = 5.5 mm

It is worth noting that the strain process in these models is essentially different. Figure 14, local extremes of the bending curve in the bimorph correspond to the location of electrodes on piezo ceramics. Meanwhile, local sections with maximum curvature of the bending curve in the unimorph are located opposite the clearances between the piezo elements. Therefore, the effect of formation of annular waves here is more pronounced.

This research used analytics and numerical methods to examine the models of bimorph and unimorph disk piezo actuators with five ring piezo elements. It compared the shapes of depressions and their maximum values at identical dimensions (outer diameter of 50 mm) and identical voltages on the piezo elements. Quasi-static voltages with an amplitude of 80 V changed with time according to the cosine law with a phase offset of 90° on neighboring piezo elements. At that, the thickness of the passive layer in the brass unimorph was chosen at optimal levels for the methods that was described by Li *et al.* (1999). Both piezo ceramic layers of the bimorph had an identical thickness of 0.2 mm. The generalization of the comparison of bending functions and amplitudes found that the unimorph model had the best indices for the generation of annular waves of bending strain.

The voltage amplitude of 80 V which corresponded to the field density of E_Z = 400 V/mm was chosen conservatively with a view to preserving the linear transformation of voltage into strain in case of an opposite connection of piezo elements. Experiments showed that the critical field density for certain samples of PZT piezo ceramics was 660 V/mm. In addition, the relatively low voltage guarantees the absence of possible repolarization and breach of piezo ceramics.

In order to check the developed method, we conducted comparative computations through known methods of a test model of a disk unimorph with a free surface. The model consisted of two layers with an identical diameter of 50 mm: a brass base with a thickness of 0.06 mm and a PZT-5H piezo ceramic disk with a thickness of 0.2 mm. At a voltage of U = 80 V, according to the method described in study of Li *et al.* (1999) and Jang and Kan (2007), we obtained a depression at the center W_1 = 167.3 μm, according to the method presented in study of Dong *et al.* (2007), a depression W_2 = 165.6 μm, the numerical computation using the finite element method in the ANSYS system found W_3 = 170.8 μm while according to our method, the result W_4 = 171.0 μm was closest to W_3. The greatest difference in the obtained data was about 3% which is satisfactory. In addition, the computed size of depression W_4 remains unchanged if the model is represented as consisting of several, three for instance, multilayer ring blocks of varying diameter which give 50 mm when combined while the sum of layer thicknesses in each block equals the corresponding thicknesses of the initial model.

The reliability of the obtained results can be assessed by comparing data from a similar model from study by Kamitani and Hirata (2009a) which are represented in the form of diagrams in Fig. 7, to the herein considered bimorph model. According to study of Li *et al.* (1999), the depressions of the unimorph are proportional to voltage U and the square of its diameter D. Figure 7 (curve t_8) shows that the depression amplitude of a plate with a diameter of D_1 = 30 mm on axis r = 0 equals approximately W_1 = 15 μm with a voltage amplitude of U_1 = 85 V in the system. For a diameter of D_2 = 50 mm at a voltage of U_2 = 80 V, the method of similarity is used to find the new depression amplitude of the analog model:

$$W_2 = W_1 \times (D_2/D_1)^2 \times (U_2/U_1) = 15 \times (50/30) 2 \times (80/85) = 39.22\ \mu m$$

According to the analytical method, the obtained amplitude (swing) of depression $\Delta W = |W_{min}|$ with the indicated data D_2 and U_2 is 39.4 μm while according to the finite element method -39.6 μm. In both cases, deviation from the known solution does not exceed 1%.

The dependencies of the depression on the radial coordinate of the bimorph which are shown in Fig. 6 and 7 are similar. Thus, the obtained results are correct and reliable.

Furthermore, numerical experiments found that the consideration of the rigidity of electrodes enabled increasing the accuracy of modeling by at least 10% which is important for the design of precision devices.

The optimal unimorph model which was chosen based on its electromechanical parameters does not solve all problems. Its application is limited, for instance by temperature conditions. Being a system that comprises of nonhomogeneous plates, the unimorph is sensitive to temperature changes. The differences in temperature coefficients of linear expansion even in a stationary thermal field can cause global bending or buckling of the entire multilayer system. A selection of materials can reduce this negative effect in unimorphs. Bimorphs are not exposed to temperature bending due to their symmetric placement of layers.

Figure 16 shows the graphical dependencies of the global deformations of the unimorph and bimorph when heated by 1°. The diagrams have different conditions of fastening of the outer surface of models. Curve 1 was built for a unimorph with an unfastened outer surface

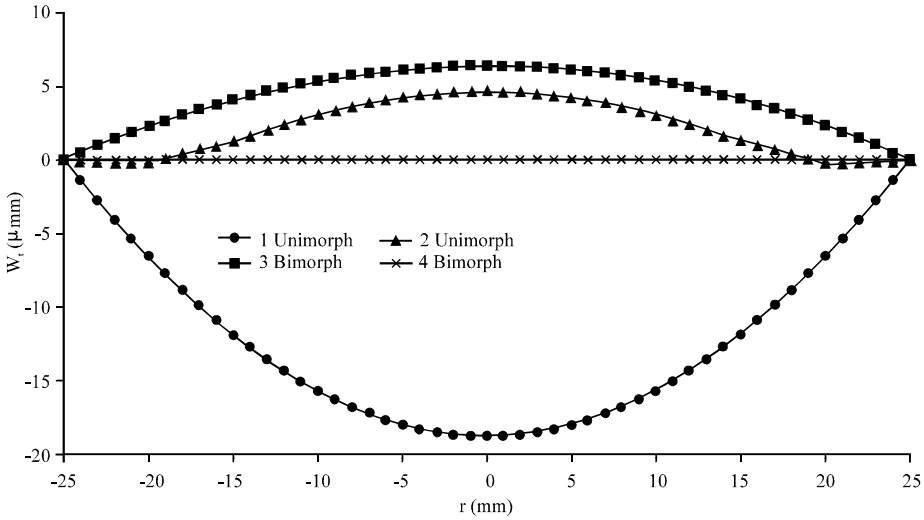

Fig. 16: Temperature deformations of the unimorph and bimorph; heating by dT = 1°

(theoretical coefficients of elastic connection were taken as $K_m = K_n = 0$). Curve 2 corresponds to the model of a uniform with a rigidly fastened surface ($K_m = K_n = 10^9$). Curve 3 shows the temperature bending of the bimorph with a fastened lower edge of the outer surface ($K_m = 0$, $K_n = 10^9$). If the surface of the bimorph is fastened rigidly or is unfastened fully, bending does not occur which is shown by line 4 which matches the zero axis.

These dependencies show that temperature deformations are commeasurable with the operating bends from the piezoeffect and depend largely on the way in which the outer surface is fastened. Rigid fastening minimizes temperature deformations in both models.

CONCLUSION

This study shows that the mechanical behavior of a bimorph and unimorph during the formation of annular strain waves is different. In the bimorph, local extremes of the bending function of the piezo disk lie in the ring zones with electrodes under voltage. In the unimorph, extremes lie in the clearances between ring piezo elements under voltage. The curvature and depressions in the unimorph clearances exceed the similar parameters of the bimorph which is why the picture of wave formation in the unimorph is more contrasting than that in the bimorph is. The results of theoretical calculations through analytical and numerical methods are virtually identical. The comparison with known designs also showed good matching.

It was found that the consideration of metal electrodes in the computational models of piezo actuators increased the accuracy of modeling by at least 10%.

The behavior of both models under changing temperature was demonstrated. The unimorph with a fastened surface bends slightly in its central part while an ideal bimorph theoretically does not deform.

The herein used original method of analytical modeling of axisymmetric multilayer piezoelectric structures with ring sections of varying rigidity with regard to temperature is universal; it generalizes specific designs that are described in other studies.

The comparative analysis of models for the generation of annular deformation waves under a stable temperature is a promising model of a unimorph structure.

ACKNOWLEDGEMENT

This study was conducted under the state order of the Ministry of Education and Science of the Russian Federation, Project No. 9.9215.2017/8.9.

REFERENCES

Anonymous, 2017. Bartels micropumps. Advance Micro Components, India.

Bar-Cohen, Y. and Z. Chang, 2000. Piezoelectrically actuated miniature peristaltic pump. Proceedings of the SPIE Conference on Smart Structures, March 6-8, 2000, Newport Beach, California, pp: 1-8.

Burdess, J.S. and T. Wren, 1986. The theory of a piezoelectric disc gyroscope. IEEE. Trans. Aerosp. Electron. Syst., 4: 410-418.

Dong, S., K. Uchino, L. Li and D. Viehland, 2007. Analytical solutions for the transverse deflection of a piezoelectric circular axisymmetric unimorph actuator. IEEE. Trans. Ultrason. Ferroelectr. Freq. Control, 54: 1240-1249.

Forster, F.K., R.L. Bardell, M.A. Afromowitz, N.R. Sharma and A. Blanchard, 1995. Design, fabrication and testing of fixed-valve micro-pumps. Proceedings of the ASME Conference on Fluids Engineering Division, November 12-17, 1995, ASME, New York, USA., pp: 39-44.

Hao, L.P., L. Ming and L.G. Jun, 2015. [A pdms based piezoelectric micro pump]. China Patent CN 104832404A, USA. (In Chinese) https://translate.google.com/translate?hl=en&sl=zh-CN&u=http://google.com/patents/CN104832404A%3Fcl%3Dpt&prev=search

He, X., J. Zhu, X. Zhang, L. Xu and S. Yang, 2017. The analysis of internal transient flow and the performance of valveless piezoelectric micropumps with planar diffuser-nozzles elements. Microsyst. Technol., 23: 23-37.

Husband, B., M. Bu, A.G. Evans and T. Melvin, 2004. Investigation for the operation of an integrated peristaltic micropump. J. Micromech. Microeng., 14: S64-S69.

Jang, L.S. and W.H. Kan, 2007. Peristaltic piezoelectric micropump system for biomedical applications. Biomed. Microdevices, 9: 619-626.

Kamitani G. and A. Hirata, 2009a. Fluid conveyance device. US. Patent US 8308454 B2, USA. http://www.google.com.pg/patents/US8308454

Kamitani, G. and A. Hirata, 2009b. Fluid conveyance device. US. Patent Application US 20090232685 A1, USA. https://www.google.com/patents/ US20090232685.

Li, X., W.Y. Shih, I. Aksay and W.H. Shih, 1999. Electromechanical behavior of PZT-brass unimorphs. J. Am.Ceram. Soc., 82: 1733-1740.

Ma, H.K., W.F. Luo and J.Y. Lin, 2015. Development of a piezoelectric micropump with novel separable design for medical applications. Sens. Actuators A Phys., 236: 57-66.

Nguyen, N.T. and S.T. Wereley, 2002. Fundamentals and Applications of Microfluidics. Artech House, Norwood, Massachusetts, USA., Pages: 454.

Pecar, B., D. Krizaj, D. Vrtacnik, D. Resnik and T. Dolzan *et al*., 2014. Piezoelectric peristaltic micropump with a single actuator. J. Micromech. Microeng., 24: 105010-105010.

Samuel, I., 2011. Gm-type piezoelectric actuator. Comput. Struct., 89: 371-379.

Shungo, K. and K. Takeshi, 2012. Piezoelectric micro pump: Murata manufacturing co. Japan Patent Office, Japan.

Timoshenko, S.P. and J. Gudier, 1979. Theory of Elasticity. 2nd Edn., Nauka, Moscow, Russia, Pages: 560.

Timoshenko, S.P. and S. Woinowsky-Krieger, 1963. Theory of Plates and Shells. 2nd Edn., State Publishing House Physico-Mathematical Literature, Moscow, Russia, Pages: 636.

Zhang, Z., J.W. Kan, S. Wang, H. Wang and J. Ma *et al*., 2016. Development of a self-sensing piezoelectric pump with a bimorph transducer. J. Intell. Mater. Syst. Struct., 27: 581-591.